Electronic Supporting Information for:

Enhancing magnetic properties of Dy(III) single-molecule magnets in octahedral coordination symmetry by tuning the equatorial ligands

Xiao-Han Peng,[a] Tao Shang,[a] Jieyu Zheng,[a, b] Ming Liu,[a] Qi Zheng,[a] and Fu-Sheng Guo*[a]

[a] Institute of Fundamental and Frontier Sciences, University of Electronic Science and Technology of China, Xiyuan Avenue 2006, Chengdu 611731 (China) E-mail: fu-sheng.guo@uestc.edu.cn
[b] Yusuf Hamied Department of Chemistry, University of Cambridge, Lensfield Road, Cambridge, CB2 1EW, UK

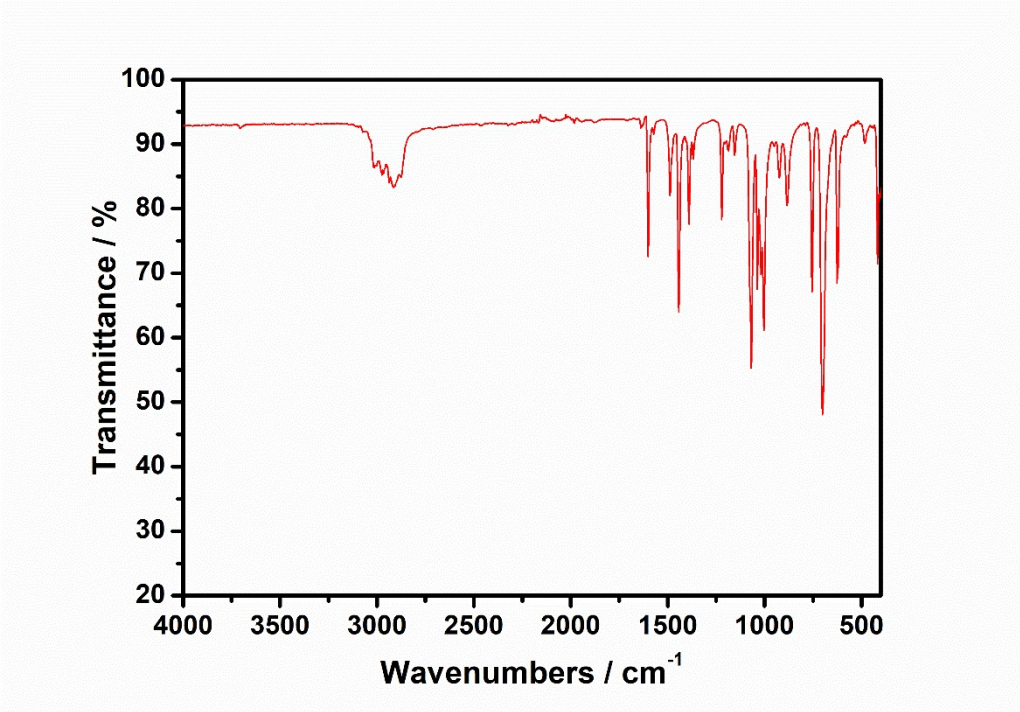

Figure S1. FT-IR spectrum of **1** under Ar atmosphere.

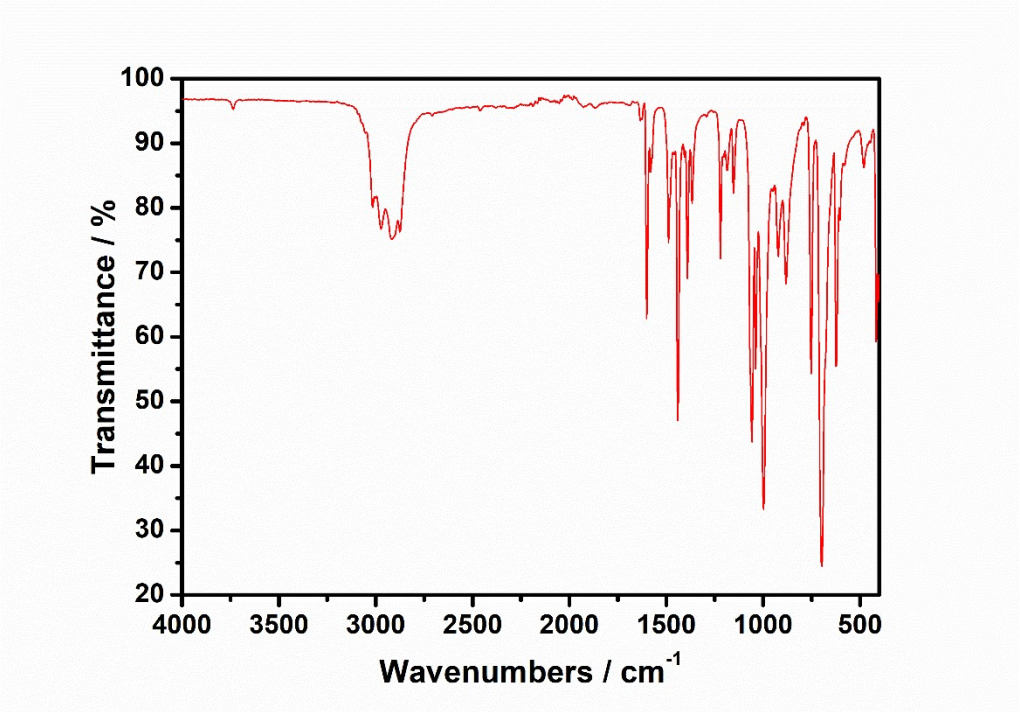

Figure S2. FT-IR spectrum of **2** under Ar atmosphere.

X-ray crystallography

Table S1. Crystal data and structure refinement for **1** and **2**.

dentification code	[Dy(OC^{t}Bu$_3$)Cl$_2$(py$_3$)] (**1**)	[Dy(OC^{t}Bu$_3$)I$_2$(py$_3$)] (**2**)
Empirical formula	$C_{28}H_{42}Cl_2DyN_3O$	$C_{28}H_{42}DyI_2N_3O$
Formula weight	670.04	852.94
Temperature/K	150.0	150
Crystal system	orthorhombic	orthorhombic
Space group	$P2_12_12_1$	$P2_12_12_1$
a/Å	8.8925(7)	9.1597(6)
b/Å	18.1625(16)	18.4547(12)
c/Å	18.7460(17)	19.0883(10)
α/°	90	90
β/°	90	90
γ/°	90	90
Volume/Å^3	3027.7(5)	3226.7(3)
Z	4	4
ρ_{calc}g/cm^3	1.470	1.756
μ/mm^{-1}	2.668	4.252
F(000)	1356.0	1644.0
Crystal size/mm^3	0.44 × 0.24 × 0.11	0.08 × 0.07 × 0.05
Radiation	MoKα (λ = 0.71073)	MoKα (λ = 0.71073)
2Θ range for data collection/°	4.486 to 53.994	4.268 to 52.992
Index ranges	-11 ≤ h ≤ 11, -23 ≤ k ≤ 21, -23 ≤ l ≤ 23	-11 ≤ h ≤ 11, -23 ≤ k ≤ 23, -23 ≤ l ≤ 23
Reflections collected	28152	31180
Independent reflections	6610 [R_{int} = 0.0538, R_{sigma} = 0.0495]	6688 [R_{int} = 0.0675, R_{sigma} = 0.0543]
Data/restraints/parameters	6610/58/365	6688/36/350
Goodness-of-fit on F^2	1.019	1.022
Final R indexes [I>=2σ (I)]	R_1 = 0.0309, wR_2 = 0.0637	R_1 = 0.0366, wR_2 = 0.0640
Final R indexes [all data]	R_1 = 0.0415, wR_2 = 0.0673	R_1 = 0.0579, wR_2 = 0.0732
Largest diff. peak/hole / e Å^{-3}	0.42/-0.59	0.71/-0.72

Table S2 Selected bond lengths (Å) and angles (deg) in complex **1** and **2**.

Bond/Angle	[Dy(OC^{t}Bu$_3$)Cl$_2$(py$_3$)] (**1**)	[Dy(OC^{t}Bu$_3$)I$_2$(py$_3$)] (**2**)
Dy1-X1	2.6158(15)	3.0324(9)
Dy1-X2	2.6398(17)	3.0690(9)
Dy1-O1	2.033(4)	2.016(6)
Dy1-N1	2.502(6)	2.507(9)
Dy1-N2	2.504(5)	2.512(8)
Dy1-N3	2.601(5)	2.597(7)
X1-Dy1-X2	161.50(6)	159.22(3)
O1-Dy1-X1	96.40(12)	96.8(2)
O1-Dy1-X2	102.06(11)	103.9(2)
O1-Dy1-N1	99.46(16)	99.8(3)
O1-Dy1-N2	94.45(16)	94.1(3)
O1-Dy1-N3	172.82(19)	173.3(4)
N1-Dy1-X1	89.57(13)	89.2(2)
N1-Dy1-X2	86.20(13)	85.1(2)
N1-Dy1-N2	165.13(17)	165.2(3)
N1-Dy1-N3	85.97(19)	85.3(3)
N2-Dy1-X1	94.12(13)	94.1(2)
N2-Dy1-X2	85.76(13)	86.7(2)
N2-Dy1-N3	80.65(18)	81.2(3)
N3-Dy1-X1	78.84(14)	78.8(2)
N3-Dy1-X2	82.89(14)	80.9(2)

Table S3 Continuous Shape Measures (CShM) calculation for **1** and **2**.

Symmetry	[Dy(OC^{t}Bu$_3$)Cl$_2$(py$_3$)]	[Dy(OC^{t}Bu$_3$)I$_2$(py$_3$)]
HP-6 (D_{6h})	33.17009	33.50472
PPY-6 (C_{5v})	26.22612	26.27611
OC-6 (O_h)	0.75769	1.96724
TPR-6 (D_{3h})	13.80195	14.13883
JPPY-5 (C_{5v})	29.3176	28.60318

Magnetic property measurements

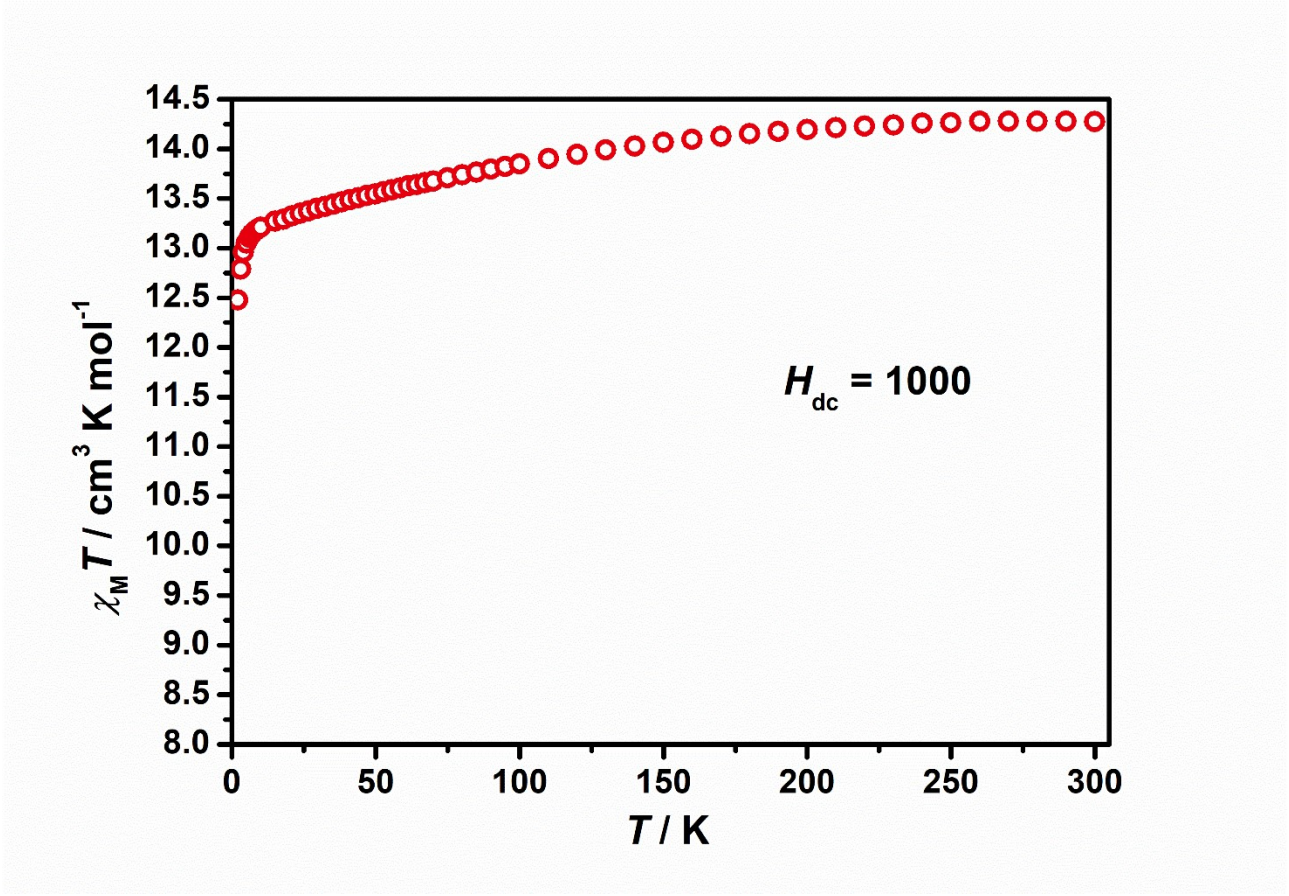

Figure S3. Measured $\chi_M T$ versus temperature (red circles) for **1** under an applied magnetic field of 1 kOe. $\chi_M T$(300 K) = 14.27 cm^3 K mol^{-1}, $\chi_M T$(2 K) = 12.4 cm^3 K mol^{-1}.

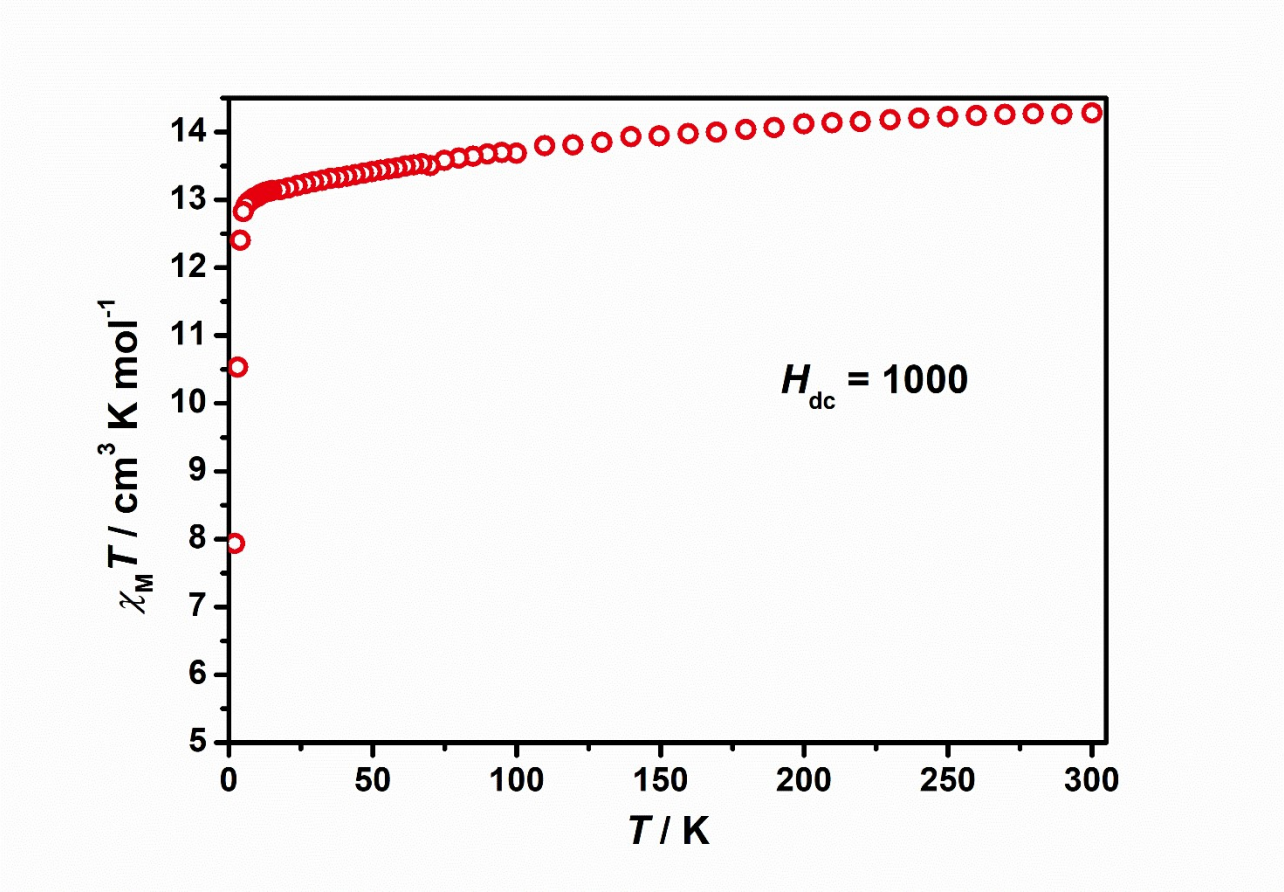

Figure S4. Measured $\chi_M T$ versus temperature (red circles) for **2** under an applied magnetic field of 1 kOe. $\chi_M T$(300 K) = 14.28 cm^3 K mol^{-1}, $\chi_M T$(2 K) = 7.93 cm^3 K mol^{-1}.

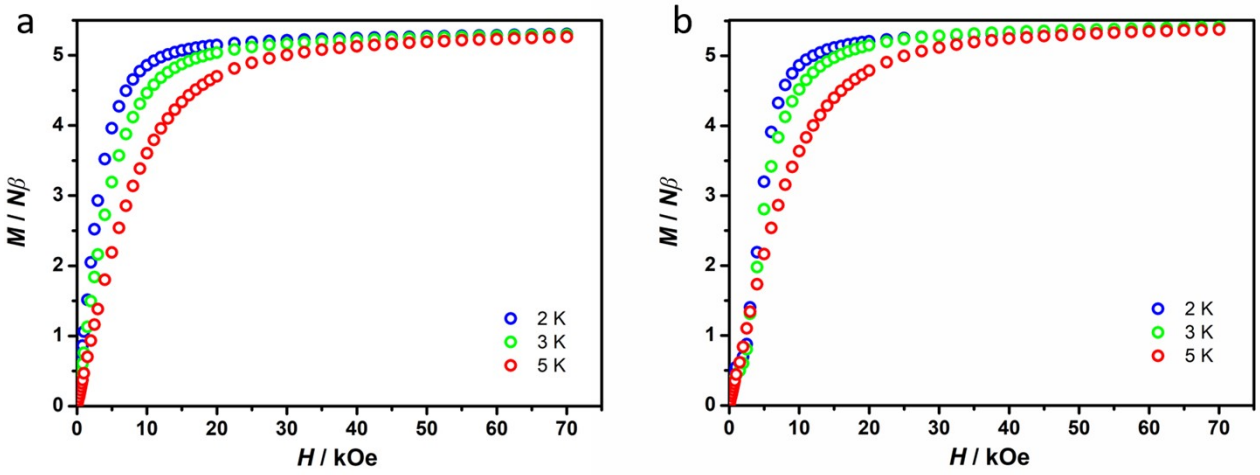

Figure S5. Variable-field magnetization data for complexes **1** (a) and **2** (b) at 2, 3 and5 K

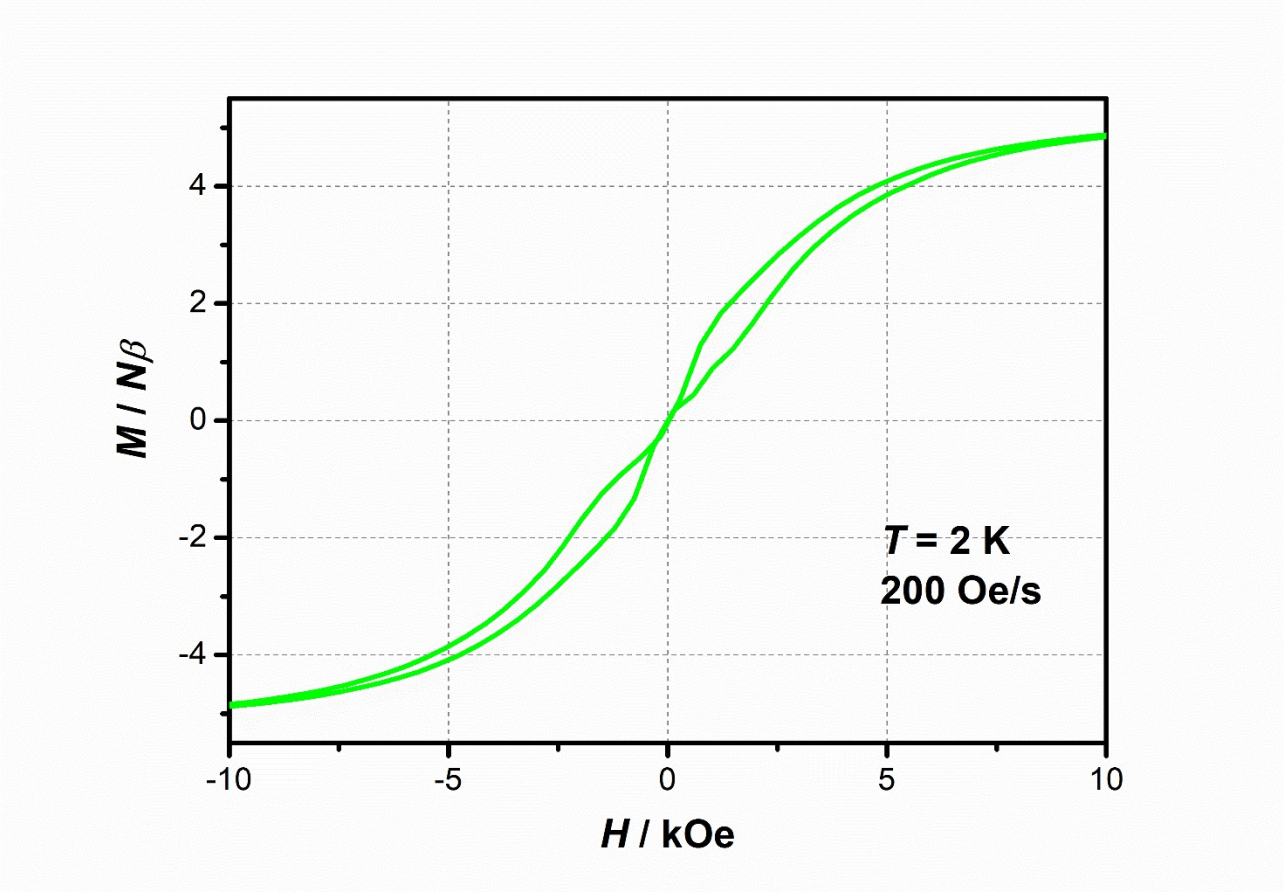

Figure S6. Magnetization vs. field hysteresis loop of **1** at 2 K using a field sweep rate of 200 Oe s^{-1}.

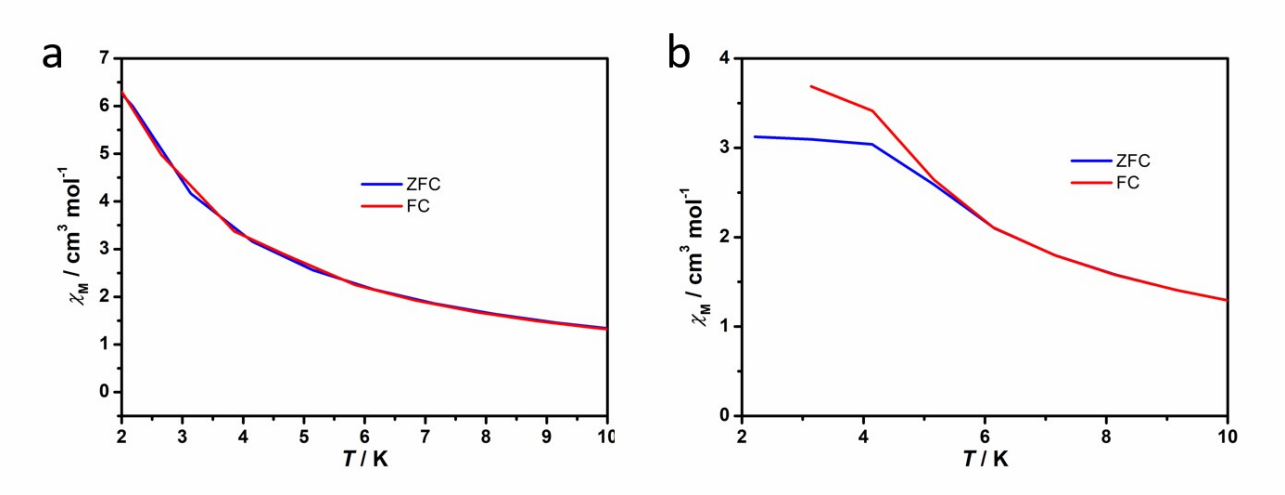

Figure S7 Zero-field-cooled/field-cooled (ZFC-FC) magnetic susceptibilities under a dc field of 1 kOe for complexes **1** (a) and **2** (b).

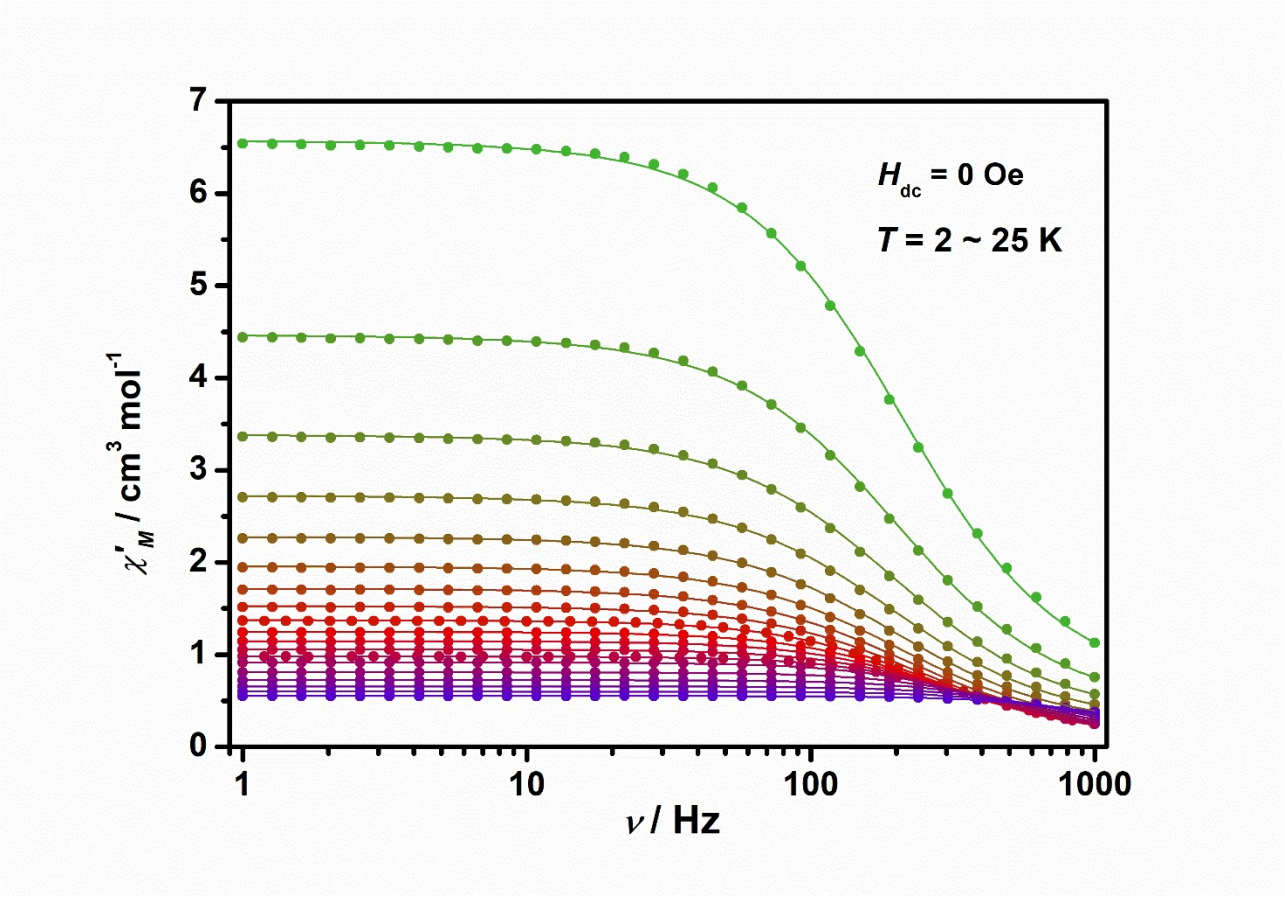

Figure S8. Frequency dependence of the in-phase susceptibility (χ'_M) for **1** under a zero DC field at AC frequencies of 0.1-1000 Hz from 2 to 70 K. Solid lines represent fits of the data using the generalized Debye model, which describe χ' and χ'' in terms of frequency, isothermal susceptibility (χ_∞), adiabatic susceptibility (χ_S), relaxation time (τ), and a variable representing the distribution of relaxation times (α).

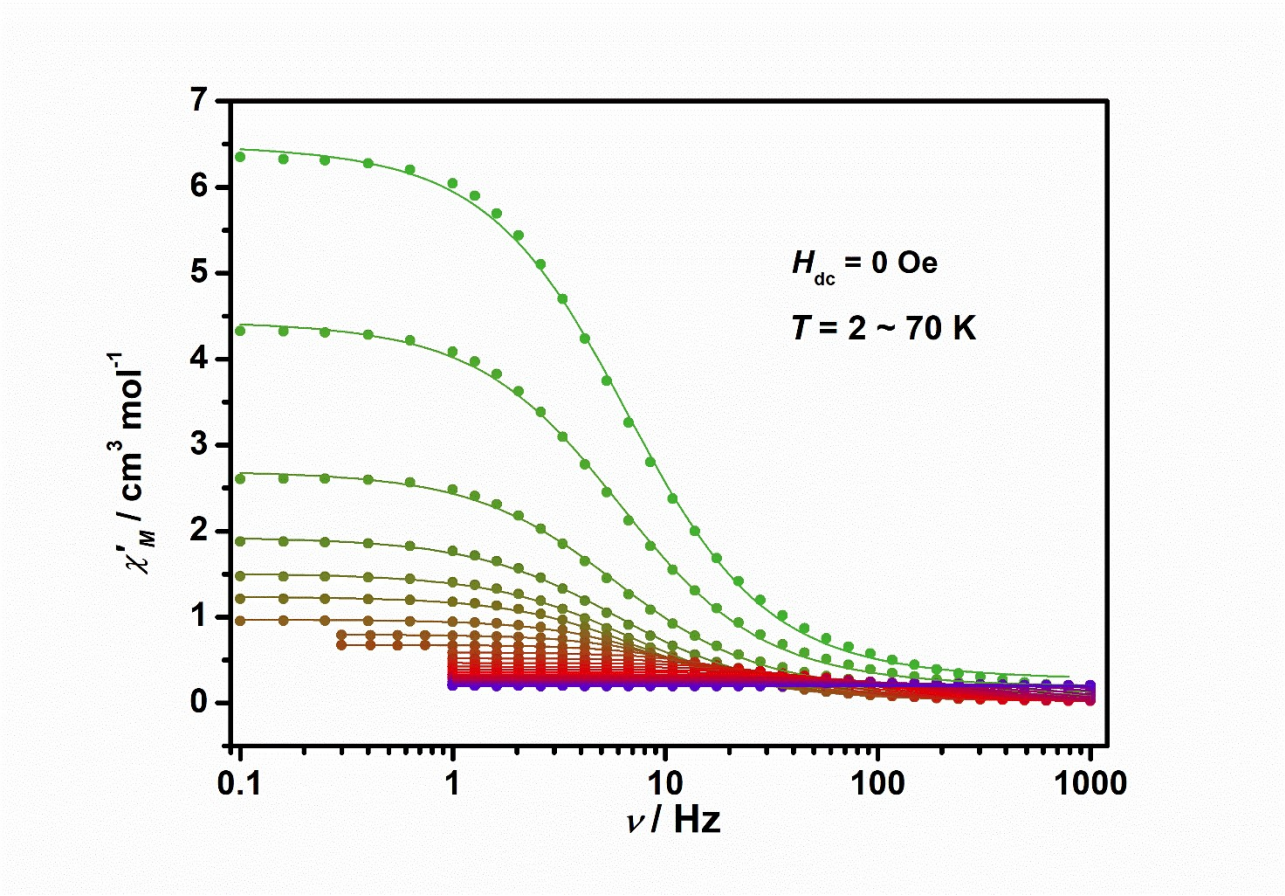

Figure S9. Frequency dependence of the in-phase susceptibility (χ'_M) for **2** under a zero DC field at AC frequencies of 0.1-999 Hz from 2 to 25 K. Solid lines represent fits of the data using the generalized Debye model, which describe χ' and χ'' in terms of frequency, isothermal susceptibility (χ_∞), adiabatic susceptibility (χ_S), relaxation time (τ), and a variable representing the distribution of relaxation times (α).

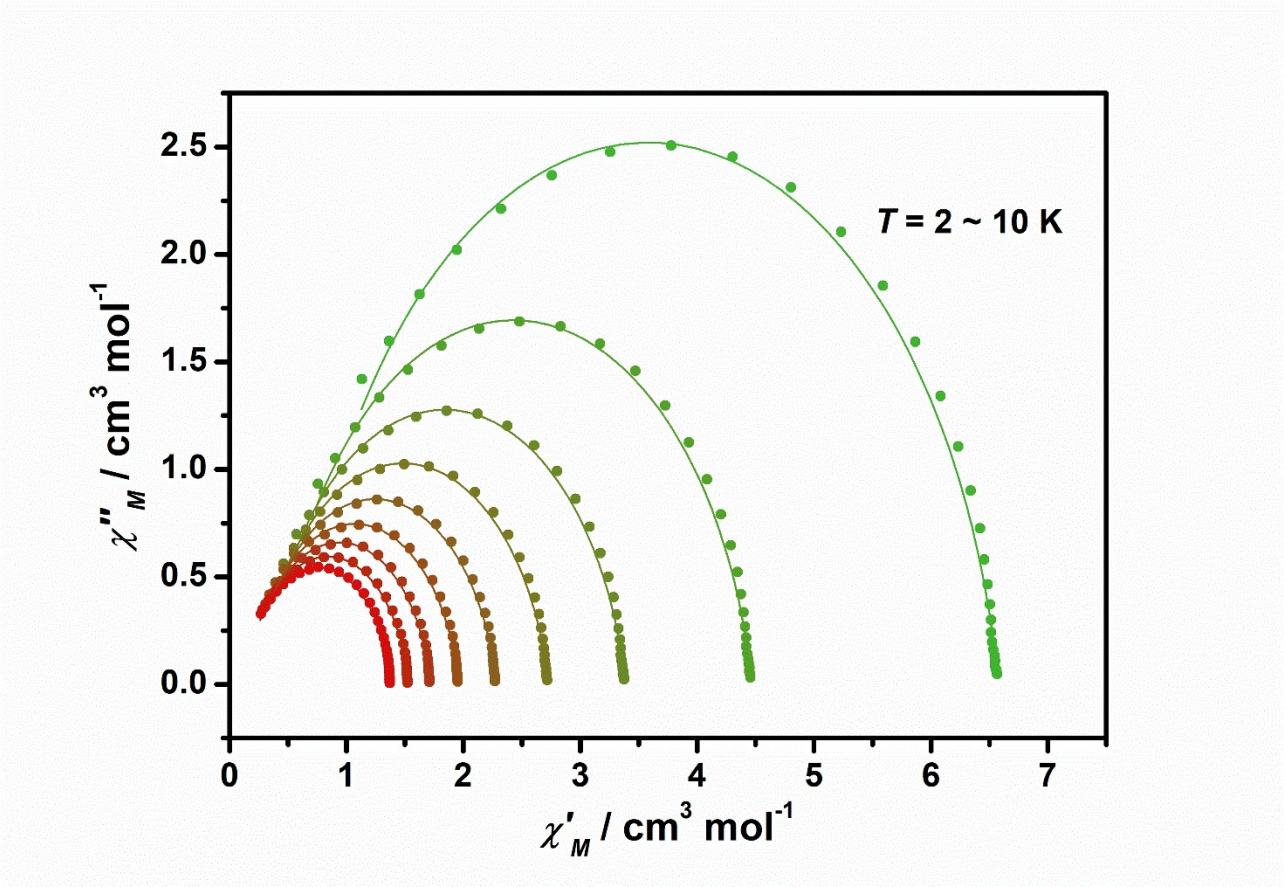

Figure S10. Cole−Cole plots for the AC susceptibilities under a zero DC field for **1** from 2-10 K. Solid lines represent fits of the data in Figure S6 using the generalized Debye model.

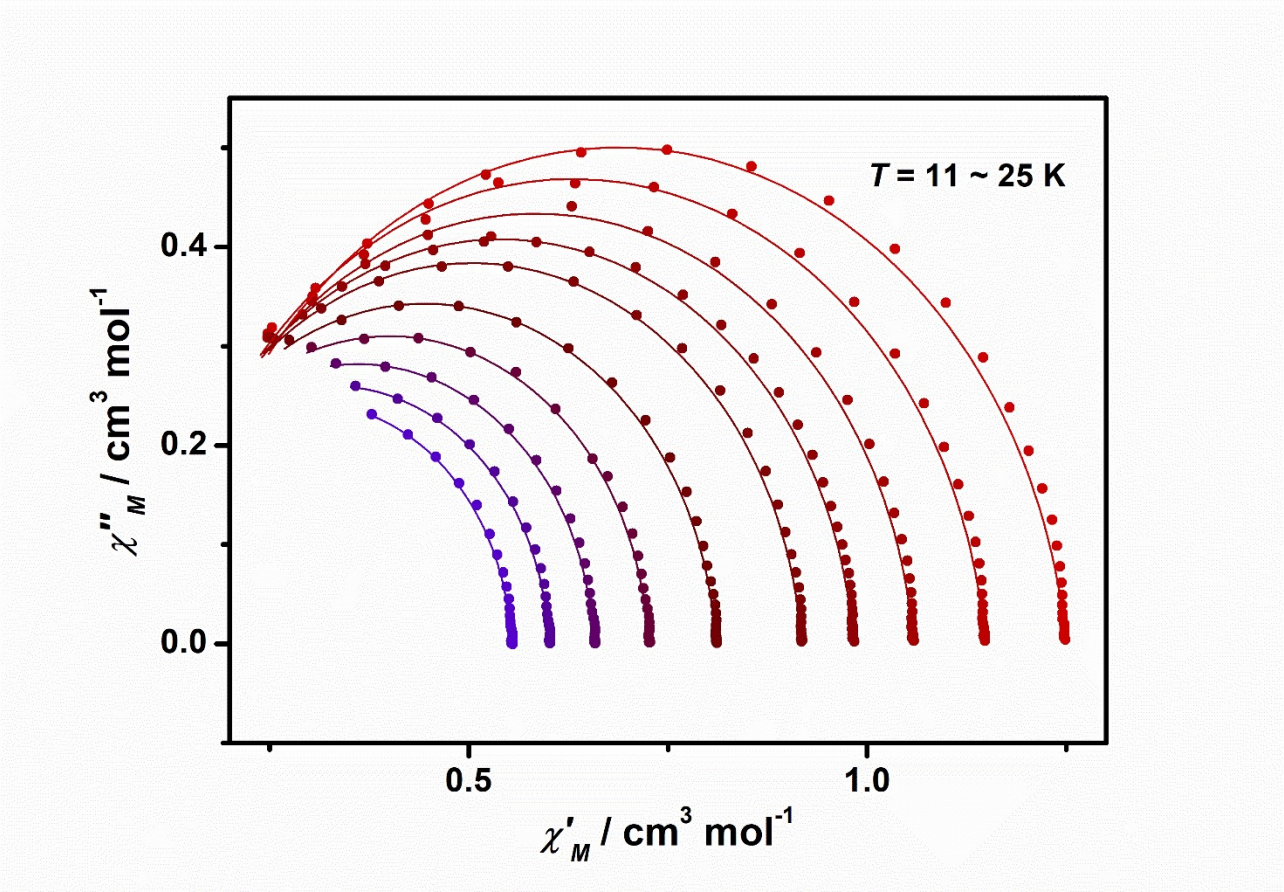

Figure S11. Cole−Cole plots for the AC susceptibilities under a zero DC field for **1** from 11-25 K. Solid lines represent fits of the data in Figure S6 using the generalized Debye model.

Table S4. Relaxation fitting parameters for **1** corresponding to Figure S10-12 using the generalized Debye model.

T / K	χ_∞ / cm^3 mol^{-1}	χ_S / cm^3 mol^{-1}	τ / s	α
2	6.57586(0.0109)	0.58392(0.03064)	7.60E-04(6.93E-06)	0.10947(0.00469)
3	4.46789(0.00778)	0.39202(0.02122)	8.02E-04(7.61E-06)	0.11683(0.00484)
4	3.38456(0.00601)	0.29784(0.01622)	8.18E-04(7.90E-06)	0.1198(0.00491)
5	2.72641(0.00488)	0.24214(0.01315)	8.20E-04(7.98E-06)	0.11999(0.00495)
6	2.27996(0.00409)	0.20572(0.01113)	8.07E-04(7.91E-06)	0.11752(0.00499)
7	1.95887(0.00349)	0.17778(0.00966)	7.80E-04(7.62E-06)	0.11211(0.00501)
8	1.71646(0.00299)	0.16206(0.00851)	7.42E-04(7.16E-06)	0.10359(0.005)
9	1.52708(0.00257)	0.1488(0.0076)	6.92E-04(6.54E-06)	0.09365(0.00495)
10	1.37462(0.00184)	0.13805(0.00581)	6.36E-04(4.92E-06)	0.08196(0.00407)
11	1.24971(0.00185)	0.12578(0.00614)	5.75E-04(5.03E-06)	0.07365(0.00462)
12	1.14791(0.00158)	0.11298(0.00564)	5.16E-04(4.35E-06)	0.06297(0.00445)
13	1.05784(0.00147)	0.10875(0.0057)	4.62E-04(4.17E-06)	0.05714(0.00469)
14	0.98226(8.10E-04)	0.09874(0.00355)	4.08E-04(2.39E-06)	0.05083(0.00294)
15	0.91706(7.40E-04)	0.09094(0.00354)	3.61E-04(2.21E-06)	0.04667(0.003)
17	0.80965(5.43E-04)	0.08017(0.00326)	2.85E-04(1.76E-06)	0.03925(0.00279)
19	0.72473(6.27E-04)	0.07525(0.00484)	2.27E-04(2.27E-06)	0.02922(0.00408)
21	0.6568(3.36EE-04)	0.0651(0.00347)	1.81E-04(1.42E-06)	0.03042(0.00277)
23	0.60026(2.71E-04)	0.05894(0.00378)	1.46E-04(1.35E-06)	0.02613(0.00283)
25	0.55295(3.15E-04)	0.04729(0.00621)	1.16E-04(1.90E-06)	0.0265(0.00417)

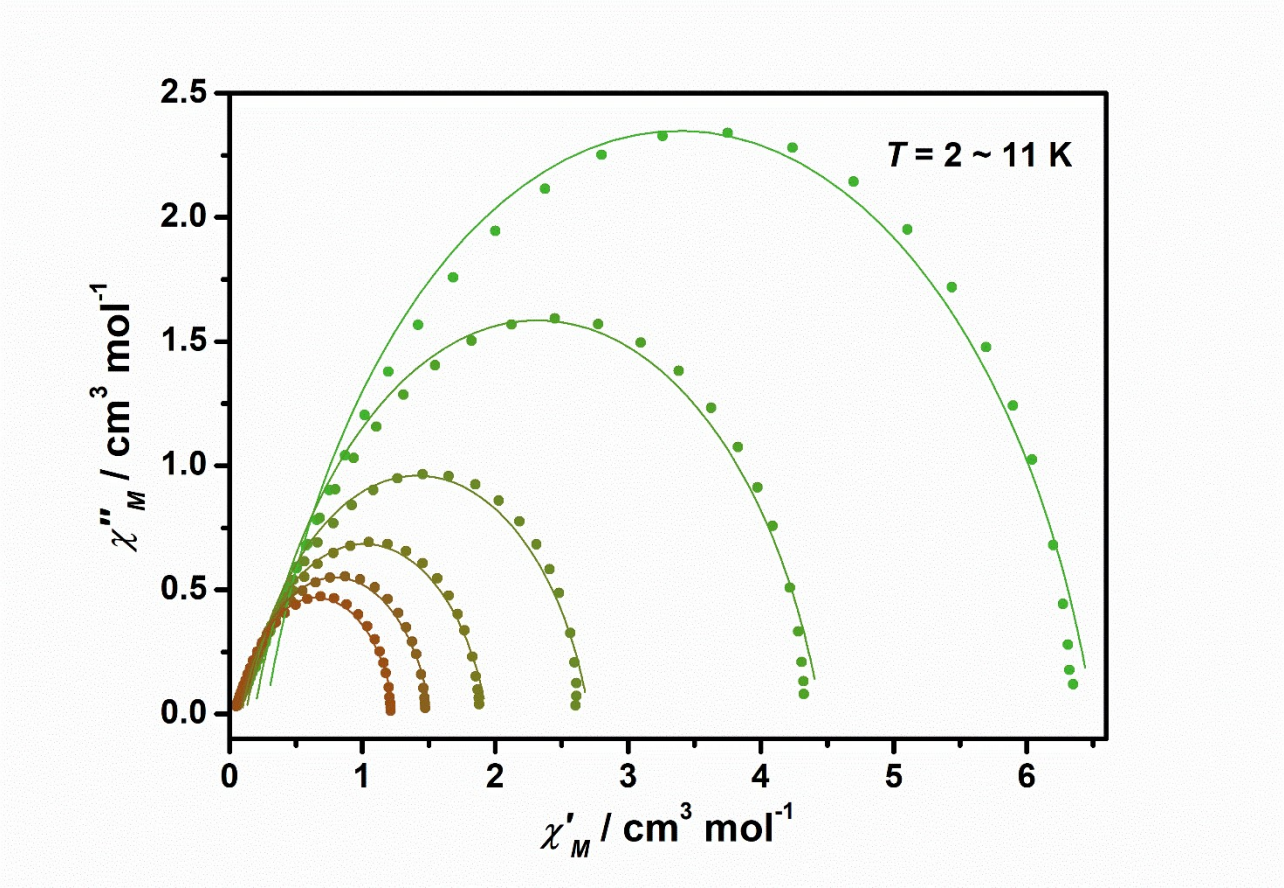

Figure S12. Cole−Cole plots for the AC susceptibilities under a zero DC field for **2** from 2-11 K. Solid lines represent fits of the data in Figure 4 using the generalized Debye model.

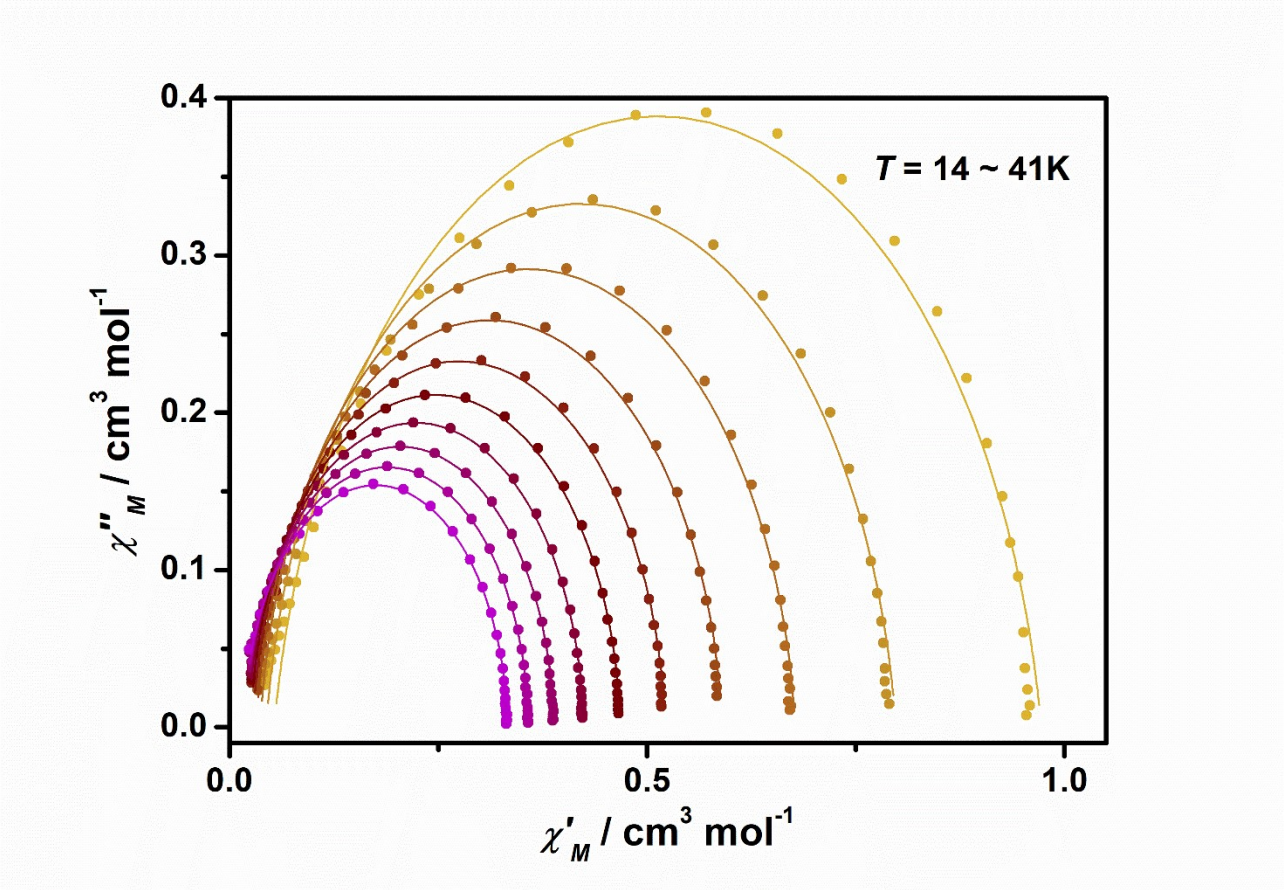

Figure S13. Cole−Cole plots for the AC susceptibilities under a zero DC field for **2** from 14-41 K. Solid lines represent fits of the data in Figure 4 using the generalized Debye model.

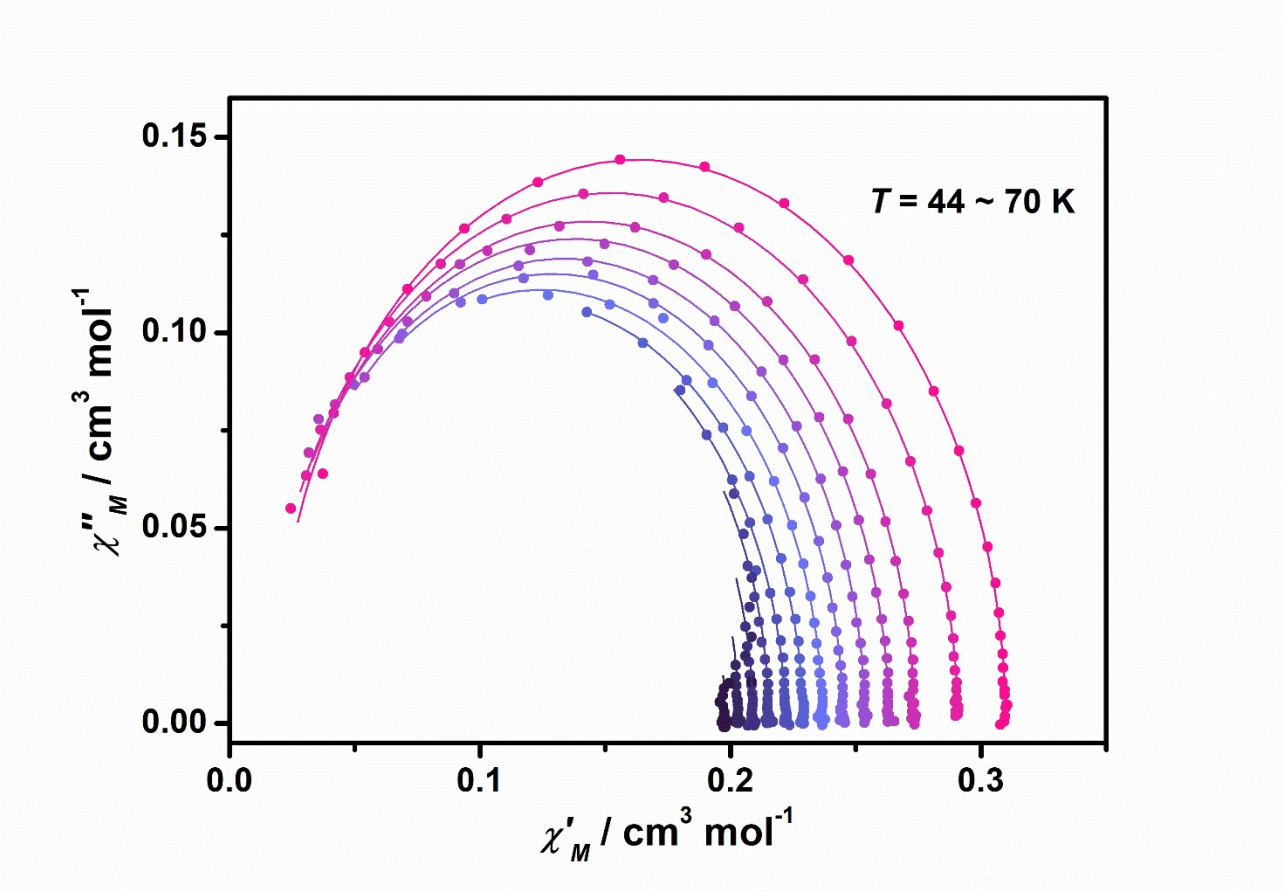

Figure S14. Cole−Cole plots for the AC susceptibilities under a zero DC field for **2** from 44-70 K. Solid lines represent fits of the data in Figure 4 using the generalized Debye model.

Table S5 Relaxation fitting parameters for **2** corresponding to Figure S13-16 using the generalized Debye model.

T / K	χ_∞ / cm^3 mol^{-1}	χ_S / cm^3 mol^{-1}	τ / s	α
2	6.50003(0.03061)	0.2721(0.02212)	0.02421(3.40E-04)	0.17716(0.00674)
3	4.45148(0.02171)	0.1853(0.01455)	0.02626(3.80E-04)	0.18604(0.00676)
5	2.70614(0.01481)	0.12225(0.00975)	0.02741(4.43E-04)	0.18607(0.00754)
7	1.93494(0.00911)	0.09048(0.00602)	0.02717(3.79E-04)	0.18645(0.00651)
9	1.51338(0.00708)	0.07519(0.00488)	0.02468(3.42E-04)	0.16869(0.0067)
11	1.24046(0.00552)	0.06519(0.00407)	0.02101(2.77E-04)	0.14297(0.00669)
14	0.9721(0.00354)	0.05332(0.00296)	0.01531(1.68E-04)	0.10609(0.00592)
17	0.79793(0.00238)	0.04385(0.00214)	0.01076(9.43E-05)	0.0792(0.005)
20	0.67729(0.00149)	0.03675(0.00153)	0.00758(5.11E-05)	0.06002(0.00396)
23	0.58982(0.00119)	0.03221(0.00115)	0.00541(2.94E-05)	0.0472(0.00334)
26	0.52157(9.08E-04)	0.02823(0.00102)	0.00392(1.96E-05)	0.03705(0.00311)
29	0.46776(5.57E-04)	0.02526(7.10E-04)	0.00291(1.05E-05)	0.02876(0.00227)
32	0.42391(4.24E-04)	0.02255(6.13E-04)	0.0022(7.02E-06)	0.02287(0.00202)
35	0.38838(3.25E-04)	0.0203(5.31E-04)	0.00171(4.80E-06)	0.01954(0.00179)
38	0.35812(2.33E-04)	0.01906(4.28E-04)	0.00135(3.11E-06)	0.01557(0.00147)
41	0.33234(2.64E-04)	0.01735(5.45E-04)	0.00108(3.22E-06)	0.01475(0.00189)
44	0.30997(2.69E-04)	0.01695(6.24E-04)	8.85E-04(3.05E-06)	0.00983(0.00219)
47	0.29086(2.22E-04)	0.01354(5.93E-04)	7.15E-04(2.35E-06)	0.01343(0.00204)
50	0.27342(1.69E-04)	0.01342(5.23E-04)	5.73E-04(1.67E-06)	0.00769(0.00177)
52	0.26333(2.09E-04)	0.01208(7.49E-04)	4.75E-04(1.97E-06)	0.00813(0.00243)
54	0.25374(1.21E-04)	0.01341(5.26E-04)	3.80E-04(1.11E-06)	0.00644(0.00161)
56	0.24492(1.07E-04)	0.01299(6.25E-04)	2.84E-04(9.88E-07)	0.00506(0.00171)
58	0.23672(1.82E-04)	0.01259(0.00161)	2.00E-04(1.84E-06)	0.00625(0.00368)
60	0.22909(1.05E-04)	0.00878(0.00176)	1.28E-04(1.34E-06)	0.01356(0.00295)
62	0.22213(1.57E-04)	0(0.00623)	7.67E-05(2.81E-06)	0.02147(0.0067)
64	0.21519(1.88E-04)	0(0.01847)	4.79E-05(5.03E-06)	0(0.01302)
66	0.20902(2.36E-04)	0(0.06054)	2.92E-05(9.97E-06)	0(0.02713)
68	0.20325(2.77E-04)	0(0.19543)	1.75E-05(1.91E-05)	0(0.05436)
70	0.19782(3.62E-04)	0(0.8101)	9.84E-06(4.39E-05)	0(0.12997)

Computational details

Complete-active-space self-consistent field (CASSCF) calculations on mononuclear complexes **1** and **2** (see Figure S1 for the calculated complete structures) on the basis of single-crystal X-ray structures have been carried out with OpenMolcas[S1] program package.

The basis sets for all atoms are atomic natural orbitals from the ANO-RCC library: ANO-RCC-VTZP for Dy^{III}; VDZP for close Cl and I; VTZ for close N and O; VDZ for distant atoms. The calculations employed the second order Douglas-Kroll-Hess Hamiltonian, where scalar relativistic contractions were taken into account in the basis set. And then, the spin-orbit couplings were handled separately in the restricted active space state interaction (RASSI-SO) procedure[S2-S3]. Active electrons in 7 active orbitals include all *f* electrons (CAS (9 in 7) in the CASSCF calculation. To exclude all the doubts, we calculated all the roots in the active space. We have mixed the maximum number of spin-free state which was possible with our hardware (all from 21 sextets, 128 from 224 quadruplets, 130 from 490 doublets). SINGLE_ANISO[S4–S6] program was used to obtain the energy levels, ***g*** tensors, magnetic axes, *et al.* based on the above CASSCF/RASSI-SO calculations.

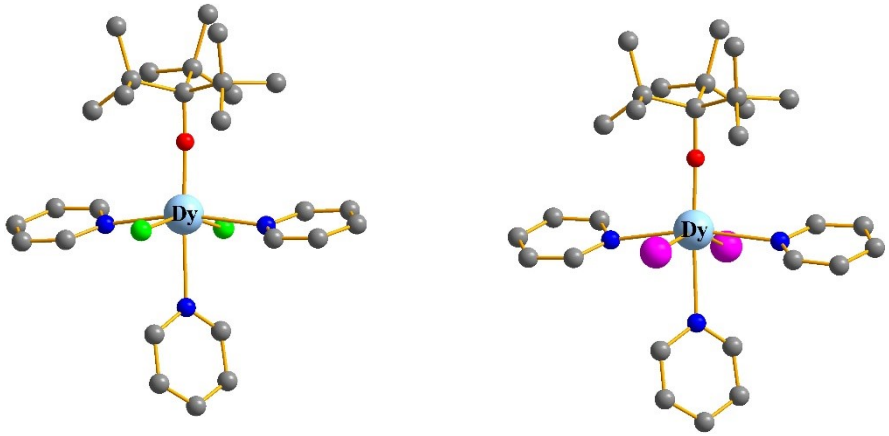

1 **2**

Figure S15. Calculated complete structures of complexes **1** and **2**. H atoms are omitted for clarify.

Table S6. Calculated energy levels (cm^{-1}), $\boldsymbol{g}$ (g_x, g_y, g_z) tensors and predominant m_J values of the lowest eight Kramers doublets (KDs) of complexes **1** and **2** using CASSCF/RASSI-SO with OpenMolcas.

KDs	**1**			**2**		
	E	***g***	m_J	*E*	***g***	m_J
1	0.0	0.009 0.013 19.837	±15/2	0.0	0.001 0.001 19.879	±15/2
2	319.3	0.391 0.678 16.558	±13/2	374.7	0.020 0.024 17.004	±13/2
3	489.2	3.516 4.958 12.823	±11/2	651.1	0.205 0.239 13.876	±11/2
4	584.8	7.932 5.699 0.338	±7/2	771.0	3.132 3.517 14.394	±9/2
5	703.6	2.000 2.756 11.051	±3/2	841.5	8.380 4.939 1.251	±7/2
6	732.9	0.137 1.993 17.245	±1/2	903.2	1.274 3.873 14.945	±3/2
7	768.5	1.085 1.300 17.130	±5/2	973.6	0.124 0.963 17.312	±1/2
8	828.5	0.136 0.307 19.088	±9/2	1025.5	0.272 1.012 18.041	±5/2

Table S7. Wave functions with definite projection of the total moment | m_J > for the lowest eight KDs for complexes **1** and **2** using CASSCF/RASSI-SO with OpenMolcas.

	E/cm^{-1}	wave functions
1	0.0	99.5%|±15/2>
	319.3	94.5%|±13/2>
	489.2	35.2%|±11/2>+22.6%|±3/2>+17.9%|±1/2>+10.1%|±7/2>+6.6%|±5/2>
	584.8	51.3%|±11/2>+24.1%|±1/2>+12.5%|±9/2>+9.2%|±5/2>
	703.6	46.2%|±9/2>+21.0%|±3/2>+14.9%|±7/2>+8.5%|±11/2>
	732.9	26.5%|±1/2>+25.8%|±5/2>+22.2%|±3/2>+16.3%|±7/2>
	768.5	26.8%|±7/2>+24.8%|±5/2>+18.3%|±9/2>+16.3%|±3/2>+11.6%|±1/2>
	828.5	30.9%|±7/2>+26.7%|±5/2>+16.9%|±3/2>+14.5%|±1/2>+9.4%|±9/2>
2	0.0	99.9%|±15/2>
	374.7	99.3%|±13/2>
	651.1	93.2%|±11/2>
	771.0	37.6%|±1/2>+27.5%|±9/2>+14.4%|±5/2>+11.1%|±3/2>
	841.5	52.7%|±9/2>+24.9%|±3/2>+11.9%|±7/2>+8.0%|±1/2>
	903.2	42.5%|±7/2>+41.6%|±5/2>+9.0%|±3/2>
	973.6	41.6%|±1/2>+27.9%|±3/2>+12.0%|±7/2>+12.0%|±9/2>
	1025.5	38.3%|±5/2>+25.3%|±7/2>+22.6%|±3/2>+10.5%|±1/2>

Table S8. LoProp charge of each atom corresponding to complexes **1** and **2**.

	Dy1	X1	X2	O1	N1	N2	N3
1	2.4108	-0.8556	-0.8611	-1.0559	-0.3814	-0.3839	-0.3435
2	2.3353	-0.8199	-0.8101	-1.0652	-0.3895	-0.3923	-0.3657

The theoretically predicted effective barrier as a function of temperature has the form[S7,S8]

$$U_{eff}(T) = \sum_{i=1}^{n} \frac{K_i(T)}{N} E_i \qquad \text{(S1)}$$

$$N = \sum_i k_i(T) \qquad \text{(S2)}$$

Each KD has a particular demagnetization rate which is:

$$K_i(T) = \frac{\exp(-E_i / k_B T)}{Z} k_{QT,i} \qquad \text{(S3)}$$

Where i is the index of each KD, E_i represents the doublet energy obtained through CASSCF calculations, $Z = \sum_i exp(-E_i/k_B T)$ is the partition function, k_B is the Boltzmann constant, and $k_{QT,i} = \frac{g_{XY,i}^2}{2\sqrt{g_{XY,i}^2 + g_{Z,i}^2}}$ is the tunneling relaxation rate for doublet i. The coefficient $\frac{K_i(T)}{\sum_i K_i(T)}$ before E_i in equation (S1) represents the relative contribution of corresponding KD to relaxation.

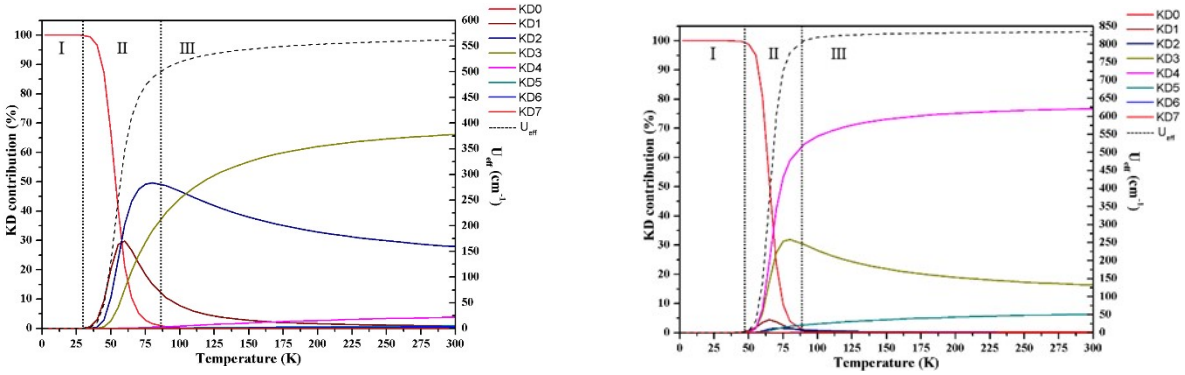

1 **2**

Figure S16 Predicted effective energy barriers and relaxation contributions from various KDs of complexes **1** and **2**. U_{eff} is represented as a dashed black line, and its value is indicated on the right y-axis. The left y-axis represents the relative contribution of each KD to relaxation.

According to the method for the prediction of tunneling demagnetization time (τ_{QTM}) proposed by Aravena *et al.*,[S7,S8] we calculated the value of τ_{QTM} according to equations (S4)–(S5).

$$\tau_{QTM} = \frac{1}{2k} \qquad \text{(S4)}$$

$$k = \frac{\beta B_{ave}}{h} \cdot \frac{g_{XY}^2}{2(g_{XY}^2 + g_Z^2)^{\frac{1}{2}}} \qquad \text{(S5)}$$

Where $g_{XY}^2 = (g_X^2 + g_Y^2)$, k is the rate of ground state QTM. As usual, the magnitude of the magnetic fields, arising

from both dipolar and hyperfine interactions, is of a few tens of mini-Tesla (mT). Thus, in this work, B_{ave} is set to be 20 mT.

Table S9. Values of B_{ave}, principal values of the ***g***-tensor of the lowest KD and the QTM time (τ_{QTM}).

Compound	B_{ave} (mT)	g_X	g_Y	g_Z	τ_{QTM} (s)
2	20	0.8576×10^{-3}	0.1304×10^{-2}	19.8372	2.91×10^{-4}
1	20	0.1136×10^{-3}	0.1411×10^{-3}	19.8791	2.16×10^{-2}

Table S10 Weight of calculated crystal-field parameter B (k, q) of complexes **1** and **2**.

B (k, q)		**1**	**2**
k	q		
2	0	30.57%	38.42%
4	0	14.03%	12.86%
6	0	2.46%	2.82%
2	–2	2.18%	0.88%
2	–1	4.04%	2.68%
2	1	1.51%	2.13%
2	2	11.67%	8.09%
4	–4	0.37%	0.47%
4	–3	0.04%	0.50%
4	–2	1.13%	0.96%
4	–1	3.16%	2.38%
4	1	1.58%	1.94%
4	2	0.72%	2.89%
4	3	0.69%	1.05%
4	4	12.70%	8.99%
6	–6	0.76%	0.10%
6	–5	1.30%	1.09%
6	–4	0.24%	0.02%
6	–3	0.08%	0.27%
6	–2	0.52%	0.57%
6	–1	0.65%	0.89%
6	1	0.79%	0.66%
6	2	0.34%	0.82%
6	3	0.45%	0.38%
6	4	3.83%	2.75%
6	5	0.64%	0.68%
6	6	2.35%	3.37%

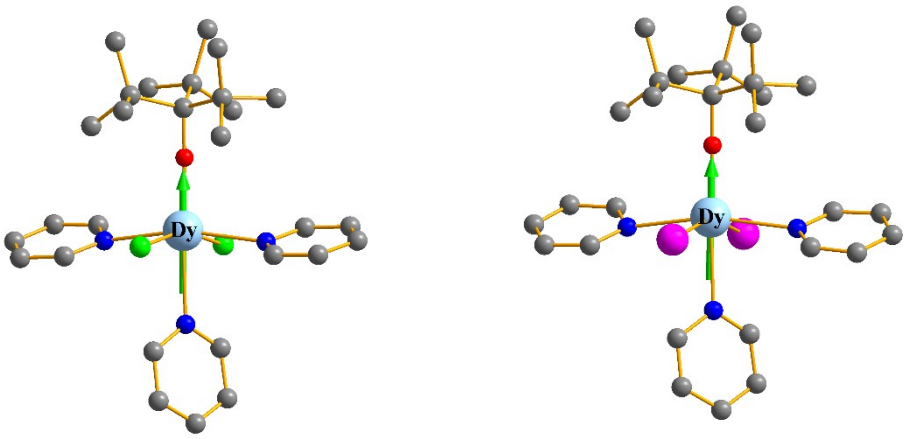

1 **2**

Figure S17 Calculated orientation of the local main magnetic axis on complexes **1** and **2**.

References:

S1 Galván, I. F.; Vacher, M.; Alavi, A.; Angeli, C.; Aquilante, F.; Autschbach, J.; Bao, J. J.; Bokarev, S. I.; Bogdanov, N. A.; Carlson, R. K.; Chibotaru, L. F.; Creutzberg, J.; Dattani, N.; Delcey, M. G.; Dong, S. S.; Dreuw, A.; Freitag, L.; Frutos, L. M.; Gagliardi, L.; Gendron, F.; Giussani, A.; González, L.; Grell, G.; Guo, M. Y.; Hoyer, C. E.; Johansson, M.; Keller, S.; Knecht, S.; Kovacevic, G.; Källman, E.; Manni, G. L.; Lundberg, M.; Ma, Y. J.; Mai, S.; Malhado, J. P.; Malmqvist, P. Å.; Marquetand, P.; Mewes, S. A.; Norell, J.; Olivucci, M.; Oppel, M.; Phung, Q. M.; Pierloot, K.; Plasser, F.; Reiher, M.; Sand, A. M.; Schapiro, I.; Sharma, P.; Stein, C. J.; Sørensen, L. K.; Truhlar, D. G.; Ugandi, M.; Ungur, L.; Valentini, A.; Vancoillie, S.; Veryazov, V.; Weser, O.; Wesołowski, T. A.; Widmark, Per-Olof.; Wouters, S.; Zech, A.; Zobel, J. P.; Lindh. R. *J. Chem. Theory Comput.* **2019**, *15*, 5925–5964.

S2 Malmqvist, P. Å.; Roos, B. O.; Schimmelpfennig, B. *Chem. Phys. Lett.,* **2002**, *357*, 230–240.

S3 Heß, B. A.; Marian, C. M.; Wahlgren, U.; Gropen, O. *Chem. Phys. Lett.,* **1996**, *251*, 365–371.

S4 Chibotaru, L. F.; Ungur, L.; Soncini, A. *Angew. Chem., Int. Ed.* **2008**, *47*, 4126–4129.

S5 Ungur, L.; Van den Heuvel, W.; Chibotaru, L. F. *New J. Chem.* **2009**, *33*, 1224–1230.

S6 Chibotaru, L. F.; Ungur, L.; Aronica, C.; Elmoll, H.; Pilet, G.; Luneau, D. *J. Am. Chem. Soc.* **2008**, *130*, 12445–12455.

S7 Daniel, A.; *J. Phys. Chem. Lett.* **2018**, *9*, 5327–5333.

S8 Yin, B.; Li, C. C.; *Phys. Chem. Chem. Phys.* **2020**, *22*, 9923–9933.